Reactivity and lifetime assessment of an oxygen releasable manganese ore with biomass fuels in a 10 kW<inf>th</inf> pilot rig for chemical looping

Downloaded from: https://research.chalmers.se, 2025-12-04 23:27 UTC

Citation for the original published paper (version of record):
Mei, D., Soleimani Salim, A., Linderholm, C. et al (2021). Reactivity and lifetime assessment of an oxygen releasable manganese ore with biomass fuels in
a 10 kW<inf>th</inf> pilot rig for chemical looping combustion. Fuel Processing Technology, 215.
http://dx.doi.org/10.1016/j.fuproc.2021.106743

N.B. When citing this work, cite the original published paper.

research.chalmers.se offers the possibility of retrieving research publications produced at Chalmers University of Technology. It covers all kind of research output: articles, dissertations, conference papers, reports etc. since 2004. research.chalmers.se is administrated and maintained by Chalmers Library

(article starts on next page)

Fuel Processing Technology 215 (2021) 106743

Contents lists available at ScienceDirect

Fuel Processing Technology

journal homepage: www.elsevier.com/locate/fuproc

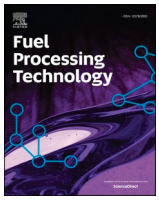

Research article

Reactivity and lifetime assessment of an oxygen releasable manganese ore with biomass fuels in a 10 kW_{th} pilot rig for chemical looping combustion

Daofeng Mei [a,b,*], Amir H. Soleimanisalim [a], Carl Linderholm [a], Anders Lyngfelt [a], Tobias Mattisson [a]

[a] Division of Energy Technology, Department of Space, Earth and Environment, Chalmers University of Technology, Gothenburg, SE 41296, Sweden
[b] College of Engineering, Huazhong Agricultural University, Wuhan 430070, China

ARTICLE INFO

Keywords:
CO_2 capture
Chemical looping combustion
Oxygen carrier
Manganese ore
Biomass solid fuels
Fluidised bed attrition

ABSTRACT

Finding a suitable oxygen carrier is crucial for the development of Chemical Looping Combustion (CLC). A new manganese ore was tested with different biomass fuels in a recently commissioned 10 kW_{th} unit. The ore maintains the capability of generating O_2 gas in N_2 after continuous operations with the fuels, however, the concentration was relatively low within 0.45–1.0 vol% at 820 to 975 °C. Influence of temperature, solids circulation and fuel power was examined for different fuels. Temperature increase enhances the carbon capture and reduces the oxygen demand, while the solids circulation and fuel power should be carefully controlled. Using biomass char the oxygen demand can be lowered to 2.6% while the carbon capture was close to 99%. The manganese ore showed a higher reactivity than the often-used ilmenite. Thus, a decrease of 8–10% in oxygen demand was achieved by using the manganese ore in comparison to ilmenite. During the 42 h of hot operation, defluidisation was not observed. Based on the analysis of the 35 fine samples collected, the initial attrition after first hours of operation was high, but gradually decreased to a relatively stable value of 0.27 and 0.12 wt%/h for hot and fuel operations, respectively, corresponding a lifetime of 370–830 h.

1. Introduction

As the most important anthropogenic greenhouse gas, the mean CO_2 concentration is increasing in the atmosphere after pre-industrial decades [1,2], which resulted in an average temperature rise of around 0.2 °C per decade [3].Thus, the elimination of CO_2 emissions is critical for preventing the increase of global temperature over the 1.5–2 °C danger line [4,5]. Carbon Capture and Storage (CCS) is one of the most cost-effective ways to reach this target by capturing and sequestrating the CO_2 emitted from power plants and industrial facilities into underground aquifers or depleted oil/gas fields [4]. Chemical Looping Combustion (CLC) offers a combustion process with potentially much lower costs than competing technologies for CO_2 capture, i.e. pre-, post- and oxyfuel combustion, attributable to the features of intrinsic CO_2 capture and avoidance of costly gas separation units [6–10].

In CLC technology, the conventional combustor is split into an air reactor and a fuel reactor, while the oxygen for fuel combustion is transported by an oxygen carrier circulating between the two reactors [11]. As seen in Fig. 1, the oxygen carrier, with MeO_x and MeO_{x-1} as oxidised and reduced form, respectively, is usually a metal oxide based on Fe, Cu, Mn, Ni and/or perovskite [12–14]. The combustion mechanism of fuel, e.g. coal and biomass solid fuel, in the fuel reactor can be different depending mainly on the properties of the oxygen carrier [15–17] and the reacting environment [18]. It has been shown that the mode of oxygen transfer can differ, and oxygen carriers can react via normal CLC, in addition to Chemical Looping with Oxygen Uncoupling (CLOU) [15,19]. For normal CLC process, the solid fuel is rapidly decomposed to char and volatiles via reaction (r.1) after entering the fuel reactor. The char from pyrolysis is then gasified by steam to CO and H_2 via the gasification reaction (r.2). Subsequently, the mixture of volatiles and gasification products is converted to CO_2 and H_2O by MeO_x through reaction (r.3), while the oxygen carrier is reduced to MeO_{x-1}. Furthermore, the normal CLC can be changed to CLOU mode [19] using specific oxygen carriers that can release gaseous O_2, such as some Cu-, Mn- and perovskite-based materials [15,20]. In this latter case, the fuel reactor has an environment with a fraction of O_2 gas because of the

* Corresponding author at: Division of Energy Technology, Department of Space, Earth and Environment, Chalmers University of Technology, Gothenburg, SE 41296, Sweden.
E-mail address: daofeng.mei@chalmers.se (D. Mei).

https://doi.org/10.1016/j.fuproc.2021.106743
Received 16 October 2020; Received in revised form 23 December 2020; Accepted 17 January 2021
Available online 3 February 2021
0378-3820/© 2021 The Authors. Published by Elsevier B.V. This is an open access article under the CC BY license (http://creativecommons.org/licenses/by/4.0/).

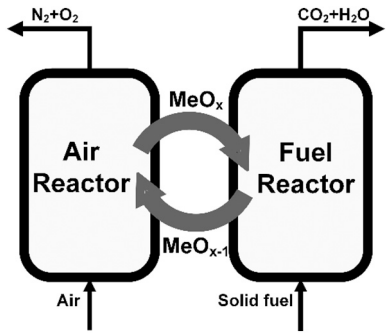

Fig. 1. Schematic diagram of chemical looping combustion with solid fuel.

decomposition of MeO_x via reaction (r.4). Therefore, in CLOU mode solid fuels can burn directly with gas phase O_2, as seen in reaction (r.5), which shows a much higher rate of fuel combustion than the normal CLC mode [21,22]. In both modes, highly concentrated CO_2 mixed with H_2O can be obtained in the gas stream leaving the fuel reactor as seen in reactions (r.3) and (r.5), respectively. The reduced oxygen carrier, MeO_{x-1}, is then conveyed to the air reactor to oxidise back to MeO_x via reaction (r.6). As seen, the combustion of solid fuel in CLC is accomplished without the mixing by air, thus, the effluent gas from the air reactor is composed by N_2 and depleted O_2, while there is ideally only CO_2 and H_2O from the fuel reactor, as shown in Fig. 1. In this case, the CO_2 can be easily separated from the fuel-reactor gas after simple and low-cost steam (H_2O) condensation. Therefore, CLC is a combustion technology which features inherent and low-energy-penalty CO_2 capture. Further, by using biomass fuels in CLC, i.e. Bio-CLC, the CO_2 fixed by photosynthesis of plants is captured and sequestrated, which leads to negative emissions of CO_2 through Biomass Energy with Carbon Capture and Storage (BECCS) technology [23,24].

Fuel reactor (CLC mode)

$$\text{Solid fuel} \rightarrow \text{Char} + \text{Volatiles} \quad \text{(r.1)}$$

$$\text{Char} + H_2O \rightarrow CO + H_2 + \text{Ash} \quad \text{(r.2)}$$

$$\text{Volatiles}, CO, H_2 + MeO_x \rightarrow MeO_{x-1} + CO_2 + H_2O \quad \text{(r.3)}$$

Fuel reactor (CLOU mode)

$$MeO_x \rightarrow MeO_{x-1} + 0.5O_2 \quad \text{(r.4)}$$

$$\text{Solid fuel} + O_2 \rightarrow CO_2 + H_2O + \text{Ash} \quad \text{(r.5)}$$

Air reactor

$$MeO_{x-1} + 0.5O_2 \rightarrow MeO_x \quad \text{(r.6)}$$

The functionality of the oxygen carrier is a cornerstone for the development of CLC technology, because it is needed for the oxygen transfer. For solid fuels, the ash after combustion has to be regularly removed from the fuel reactor in large-scale CLC systems, which will also lead to losses of oxygen carrier, thus low-cost materials such as natural ores and industrial by-products are preferred [25–31]. A number of such materials have been demonstrated for their viability in CLC, which include operations of >1524 h with ilmenite, >1075 h with iron ore, >735 h with manganese ore and > 75 h with $CaSO_4$ based oxygen carriers [8]. Among them, manganese ores showed higher reactivity than either ilmenite or iron ore [32–34], as well as the avoidance of the risk of sulphur release from $CaSO_4$-based materials [35–38]. Therefore, the interest for using manganese ores as oxygen carrier is growing [39–45]. Normally, manganese ores are composed of oxides of Mn, Fe and other minor elements. Because of the potential for releasing gaseous O_2 from $(Mn_xFe_{1-x})_2O_3$ bixbyite [15,20,46–48], several studies of manganese ores looked at the CLOU properties for such materials [33,34,49,50]. In general, a significant amount of O_2 gas can be released from some manganese ores in the first exposure to an inert gas environment, however, this behaviour usually becomes extremely weak after one or very few cycles [33,51]. Thus, an oxygen transport capacity of only 0.01–0.03 wt% corresponds to the gaseous O_2 release in CLOU mode for many manganese ores. The rate of O_2 release was relatively very low in inert gas environment [33,52,53], i.e. only 1–3% of that for Cu- based materials [18,54], however, it can be considerably improved by increasing the driving force for O_2 release using char as fuel [55]. Although the addition of $Ca(OH)_2$ was attempted to enhance the CLOU performance of some manganese ores, the resulting improvements were not significant [56]. Despite the low effect of CLOU, manganese ores showed higher reactivity than ilmenite and iron ores, especially for char gasification in CLC with solid fuels [32,57,58], which is possibly a result of catalytic effect of alkali elements [32,57,59]. Several manganese ores were subject to tests in continuous units with solid fuels. Conversion of intermediate fuel gases were greatly improved as compared to ilmenite [60–62], which leads to a significant decrease of oxygen demand for the fuel reactor gas [41,61,62] being the lowest as 4.5% [41]. The challenge for the use of these manganese ores is their attrition rate, which can vary considerably [63]. Pilot operation indicates reasonable lifetime could be possible, e.g. 100–400 h [61,62], further, it can be extended a little by sintering [42,43] or addition of foreign ions [64]. Therefore, finding manganese ores with high reactivity and sufficient mechanical properties as oxygen carrier is relevant for the development of CLC with solid fuels. The fact that manganese ores have variable composition depending upon origin, which can include significant fractions of important elements, such as Fe, Ca and Si, could explain some of the differences seen in CLOU activity and reactivity. This also means that it could be possible to find a suitable composition in nature, something which could be quite interesting for the technology.

This work tests a new manganese ore as oxygen carrier in a recently commissioned 10 kW_{th} unit for CLC with solid fuels. The CLOU behaviour, i.e. release of gas-phase O_2 in N_2 environment, was closely monitored as a function of operation time at different temperatures. Using various biomass-based solid fuels, the operation conditions including temperature, solids circulation and fuel power, was changed in a wide range to assess the CLC performance of this new oxygen carrier. Under similar conditions, the reactivity of the manganese ore was compared with the benchmark ilmenite material based on the gas conversion and the oxygen demand obtained from the experiments. Fines produced by the manganese ore particles were collected from different parts of the 10 kW_{th} unit, from which the attrition rate and lifetime of the new material were estimated as a function of operation time.

2. Experimental

2.1. Oxygen carriers

Two naturally occurred minerals, namely manganese ore and ilmenite, were compared in this work, where the ilmenite was used as a reference material [65], because of its good performance according to the investigations by various groups around the world [66–70]. Experiments in the 10 kW_{th} unit were separately carried out with these two oxygen carriers using the same fuels and similar operating conditions.

The manganese ore originates from Egypt and was denoted as “EB” in the present work. This material was selected for using in the 10 kW_{th} unit, because of the good performances shown by the same material in a 300 W_{th} reactor using a gaseous fuel [44]. Constituents in EB were analysed with the inductively coupled plasma sector field mass spectrometry (ICP-SFMS) technique, following an ISO standard method [71]. As seen in Table 1, the EB manganese ore has a high content of Mn, Fe and Si in addition to minor content of other elements. Molar ratio of Mn and Fe in the EB is close to Mn:Fe = 1:1, which might be advantageous for O_2 release due to the proneness of forming bixbyite structure [51]. The EB material was received in the form of particles with a nominal size of 100–400 μm. Before using in the 10 kW_{th} unit, it was subjected to a

Table 1
Mass fraction of the main elements in the calcined oxygen carriers (wt%).

	Mn	Fe	Ti	Si	Ca	Mg	Al	K	Na
EB	24.83	25.33	0.09	8.13	2.32	0.93	0.97	0.43	0.39
Ilmenite[a]	0.12	32.80	24.99	2.81	0.39	2.83	0.54	0.06	0.12

[a] Used as reference material in this work, data from a published work [65].

calcination and a wet sieving process in the laboratory to strengthen and to dedust the particles, respectively. In the calcination process, the manganese ore was heated in air from room temperature to 500 °C with a rate of 10 °C·min^{-1} and then to 950 °C at 1 °C·min^{-1}, to avoid the possible agglomeration caused by fast temperature increase. To strengthen the particles, a period of 1 h and 12 h at 500 °C and 950 °C, respectively, was maintained in the high-temperature furnace. After cooling down, the material was wet sieved with water to dedust and remove particles smaller than 90 μm and then dried in a low-temperature oven. The dried EB particles, having a median size of d50 = 183 μm and a bulk density of 1553 kg·m^{-3}, were then used as oxygen carrier in the experiments. Crushing strength of the oxygen carrier was the average value for fracturing 30 randomly selected particles [72], as determined by a digital apparatus (FGN-5, Shimpo), and was found to be 6.3 and 2.5 N for the fresh prepared and the used EB samples, respectively. The morphology of the fresh prepared, the used and the air-reactor filter EB particles were observed using a light microscope (MICRO-80150, TAGARNO).

The ilmenite, used as reference material, originates from Norway and has a high concentration of Fe and Ti, as shown in Table 1. Heat treatment of ilmenite was also done at 950 °C in air atmosphere but using a different heating-up programme, i.e. from room temperature to 500 °C and then to 950 °C both at 10 °C·min^{-1} with the durations of 2 and 12 h at the two temperatures, respectively. After dry sieving, ilmenite particles with a median size of d50 = 261 μm and a bulk density of 1900 kg·m^{-3} were used for tests in the 10 kW$_{th}$ unit [65].

2.2. Solid fuels

Three biomass-based solid fuels were used in the present work, i.e. steam cured black pellets (designated as BP), provided by Arbaflame company in Norway, a Swedish wood char (designated as SWC) and a German wood char (designated as GWC). Before the use in experiments, they were crushed and sieved to an initial median size of d50 = 1800, 3000 and 250 μm for BP, SWC and GWC, respectively. The SWC fuel could be further fragmented by the screw feeder when it is fed to the fuel reactor. According to the proximate and ultimate analysis in Table 2, BP is a high-volatile fuel with 74.2 wt% as volatiles matters, while SWC and GWC have only 16.7 wt% and 15.7 wt% volatiles, respectively. In addition, the oxygen content in BP is much higher than that in SWC and GWC, thus the lower heating value (LHV) for BP is lower. The theoretical oxygen ratio, Φ_0, defined as the stoichiometric moles of O_2 needed per mole of carbon in the fuel for full combustion, is also included for the different fuels in Table 2.

2.3. Reactor setup

Experiments were conducted in a new dual fluidised bed continuous unit with a nominal design of 10 kW$_{th}$ thermal input, shown in Fig. 2. In comparison to the previous 10 kW$_{th}$ system [42], the previously integrated carbon stripper was removed and a volatiles distributor [73] was added in this new unit. As shown in Fig. 2, the volatiles distributor is a perforated plate inside the fuel reactor, which can help the conversion of

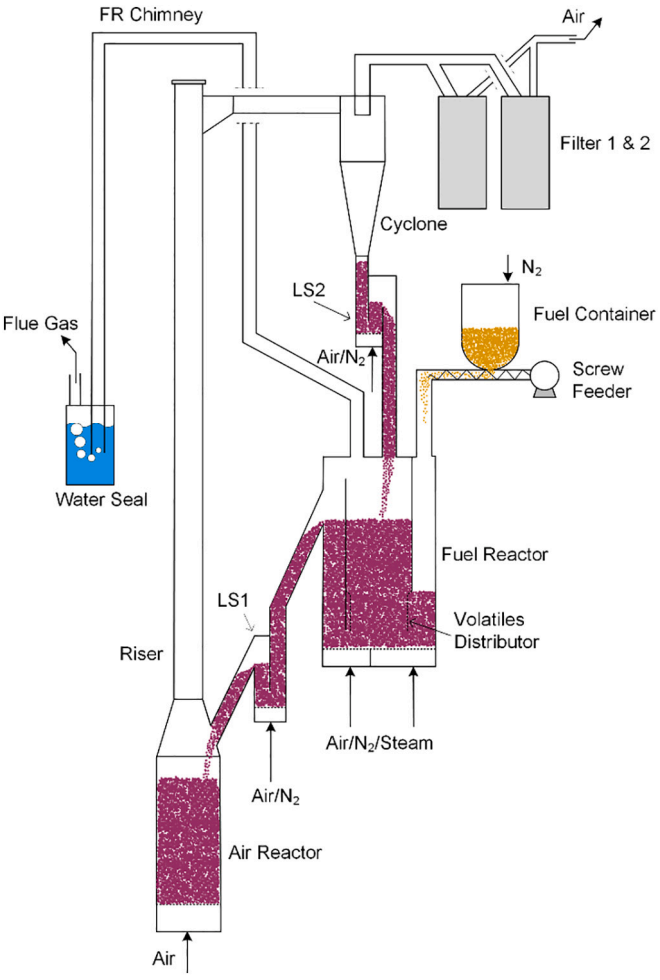

Fig. 2. Setup for the 10 kW$_{th}$ unit.

Table 2
Analysis of the solid fuels used in this work.

	Proximate (wt%, ar)				Ultimate (wt%, daf)					LHV[a] (MJ·kg^{-1})	Φ_0[b] (–)
	FC	V	M	A	C	H	N	S	O[c]		
BP	18.7	74.2	6.9	0.3	53.5	6.0	0.1	0.0	40.3	18.7	1.05
SWC	73.9	16.7	3.9	5.5	86.9	3.2	0.4	0.0	9.5	29.8	1.06
GWC	76.4	15.7	5.1	2.8	88.1	2.7	0.5	0.0	8.6	29.3	1.05

[a] Lower heating value.
[b] Stoichiometric molar ratio of O_2/C for full combustion.
[c] By difference.

volatiles by a better distribution of volatile gases [65,73]. Between the fuel and air reactor, there are a lower-position loop seal (LS1) and a higher-position loop seal (LS2), which prevent the leakage of gases between the two reactors. At the exit of the fuel reactor chimney (FR chimney), a water seal was connected to balance the pressure, while two parallel filters were used intermittently to collect the particles elutriated from the air reactor. The bed material can be fluidised with air, N_2 or steam depending on the operation conditions. Normally, during heating up and cooling down procedures, all parts of the reactor were fluidised with air. Under stable conditions, the air reactor and loop seals were always fluidised with air and N_2, respectively, while it can be selectable between N_2 and steam for the fuel reactor in CLOU and CLC tests. In the tests of O_2 release from the EB manganese ore under CLOU mode, the N_2 was used to form an inert environment. For fuel operation, the N_2 to the fuel reactor was switched to steam serving as fluidisation and gasification agent. In the process of fuel operation, the solid fuel in the fuel container was introduced into the fuel reactor by a screw feeder with the help of a known flow of N_2. As indicated in Fig. 2, the fuel falls down on a part of the bed that is separated from the main bed by a wall, which perforated to allow volatiles to enter the main bed. Here the fuel devolatilises and the remaining char mixes with the bed material and eventually reaches the main bed. After the reduction with fuel, the reduced oxygen carrier continues, via an overflow passing through the LS1, to the air reactor to be re-oxidised. The regenerated oxygen carrier particles in the air reactor were accelerated by a narrow cross-section riser and then separated in the cyclone, and finally returned to the fuel reactor via LS2 to start a new cycle. During the operation, particles from elutriation, fragmentation and/or attrition can be found at the air-reactor filters, FR chimney and water seal, which were regularly collected and analysed for the estimation of attrition rate.

The 10 kW_{th} system also includes a gas analysis unit and a data acquisition part. The gas streams leaving the reactors were continuously sampled to determine the composition. Gases from the fuel reactor were led to a gas analyser (NGA 2000, Rosemount ™) to measure the dry basis volumetric percentages of CH_4, CO, H_2, CO_2 and O_2, while the composition of air-reactor effluent gas was determined by another gas analyser (SIDOR, SICK Sensor Intelligence) for the components of CO, CO_2 and O_2. The volumetric percentage of each gas component was collected by a data logger with a rate of one point per second.

2.4. Operation condition

Totally, around 42 h of hot operation were made for the manganese ore, of which around 21 h correspond to fuel combustion, as seen in Table 3. However, because it was the first time using this material in the 10 kW_{th} unit, some unstable cases were encountered, which were excluded in the evaluation. Therefore, only stable operations are considered and discussed in this work. In addition to the EB manganese ore, two series of tests using ilmenite are also shown in Table 3 as reference cases for comparison purposes. In series 1 and 2, the release of gaseous O_2 was studied in N_2 atmosphere under a temperature rising from 500 to 820 °C and at a constant temperature of 975 °C, respectively. The tests in series 1 were performed with fresh manganese ore, i.e. before any operation with fuel, whereas the series 2 was made with the used particles after all the tests with fuels. These two series were made to see the O_2 release from fresh and used EB particles. From the fuel operation in series 3–10, the effects of fuel-reactor temperature, oxygen carrier circulation and fuel power can be evaluated, while series 11–14 were only considered for attrition evaluation. The solids circulation is controlled by the AR flow shown in Table 3, i.e. a higher air flow leads to a faster oxygen-carrier circulation. However, the circulation rate cannot be directly measured or calculated in the 10 kW_{th} unit, a circulation index is used to indicate the solids circulation in this work, as seen in Section 3 below.

In the case of ilmenite, previous operation with BP and SWC at 975 and 985 °C were used to compare and evaluate the reactivity of the EB manganese ore. The air flow to the air reactor for series 15 and 16 was varied in a small range of 180–200 $L_N \cdot min^{-1}$ to maintain a stable circulation of the ilmenite particles between reactors [65]. Prior to operation, the ilmenite had been used with different solid fuels in the same 10 kW_{th} unit [65], thus it was in an activated state [74,75].

Table 3
Operation conditions used in this work.

Series	Fuel	T_{FR} (°C)	FR gas	AR flow ($L_N \cdot min^{-1}$)	Fuel power (kW_{th})	Duration (min)
EB manganese ore						
1[a]		500–820	N_2	200	0	150
2[a]		975	N_2	200	0	57
3	BP	820–975	H_2O	150–300	6.0	652
4	BP	920	H_2O	200	8.0	17
5	BP	920	H_2O	200–340	4.0	18
6	SWC	985	H_2O	130–200	6.0	75
7	SWC	820–975	H_2O	200	1.8	93
8	SWC	920–975	H_2O	200	2.7	27
9	SWC	920–975	H_2O	200	5.3	21
10	GWC	820–975	H_2O	200	6.0	210
11[b]	GWC	975	H_2O	200	9.0	26
12[b]	GWC	820	H_2O	200	5.0–9.0	43
13[b]	GWC	875	H_2O	200	5.0	17
14[b]	GWC	920	H_2O	200	5.0–9.0	32
Ilmenite[c]						
15	BP	975	H_2O	190–200	6.0	53
16	SWC	985	H_2O	180–200	6.0	51

[a] For O_2 release tests.
[b] Only considered for attrition analysis.
[c] As reference cases with data from a published work carried out in the same reactor [65].

3. Data evaluation

Solids circulation rate between the fuel and air reactor cannot be directly measured in the 10kW_{th} unit, however, it can be represented by a circulation index (CI) developed in a previous work [76], as seen in Eq. (1). This equation was established based on a correlation for solid flux calculation proposed for circulating-fluidised boilers [77].

$$CI = \Delta P_{riser} \cdot F_{AR,out} \cdot \frac{T_{AR} + 273}{273} \quad (1)$$

where the ΔP_{riser} (kPa) is the measured pressure drop over the riser of air reactor, $F_{AR,out}$ ($L_N \cdot min^{-1}$) represents the volumetric flow of gas leaving the air reactor calculated according to the inlet air flow, T_{AR} (°C) refers to the temperature in the air reactor. Thus, the circulation index CI has the unit of kPa·($L_N \cdot min^{-1}$).

The fuel power (P_{fuel}) means the input of thermal heat to the system with the fuel feed, which takes a unit of kW_{th} and calculated through Eq. (2).

$$P_{fuel} = \dot{m}_{fuel} \cdot LHV \cdot 10^3 \quad (2)$$

where $\dot{m}_{fuel}$ ($kg \cdot s^{-1}$) is the mass flow rate of fuel, calculated according a calibration of the screw feeder for various fuels during operation, *LHV* ($MJ \cdot kg^{-1}$) represents the lower heating value of the fuels listed in Table 2.

To compare the results from different operation conditions, the measured gas concentration for component i (i = CO, CH_4, H_2 or CO_2) from the fuel reactor was normalised by the total fraction of carbonaceous gases [43], i.e. CH_4, CO and CO_2, as seen in Eq. (3).

$$x_{i,N} = \frac{x_{i,FR}}{(x_{CH_4} + x_{CO} + x_{CO_2})_{FR}} \quad (3)$$

where $x_{i,FR}$ (vol%) represents the measured concentration of component i (i = CH_4, CO, H_2 or CO_2) from the fuel reactor and $x_{i,N}$ is the

corresponding normalised concentration. The fraction of other hydrogen carbon gases was also measured but not included for evaluation, because of their trace amount.

Using the fuel-reactor gas concentration $x_{i,FR}$ (i = CO, CH_4, H_2 or CO_2), a dimensionless oxygen demand (Ω_{OD}) can be calculated [67], as shown in Eq. (4). This parameter represents the theoretical ratio of O_2 required for completely oxidising the residual gaseous combustibles from the fuel reactor.

$$\Omega_{OD} = \frac{0.5x_{CO,FR} + 2x_{CH_4,FR} + 0.5x_{H_2,FR}}{\Phi_0\left(x_{CO,FR} + x_{CH_4,FR} + x_{CO_2,FR}\right)} \quad (4)$$

where the symbol Φ_0 represents the stoichiometric moles of O_2 needed per mole carbon for full combustion, with the values for different fuels used in this work shown in Table 2.

Carbon containing components from the outlet of fuel reactor can be finally captured in CLC process, whereas the carbonaceous gases generated in the air reactor will be released to the atmosphere. Thus, a carbon capture (η_{CC}) was defined according to the gases detected at the air reactor exit [62] to reflect the capacity of removing CO_2 from the combustion.

$$\eta_{CC} = \frac{x_{O_2,ini} - x_{O_2,AR} - x_{CO_2,AR}}{x_{O_2,ini} - x_{O_2,AR} - 0.21x_{CO_2,AR}} \quad (5)$$

where $x_{O2,ini}$ (vol%) represents the initial O_2 concentration at the outlet of air reactor before fuel operation, which is a bit less than 21 vol% considering the dilution by N_2 from LS1 and pressure measuring ports, $x_{O2,AR}$ (vol%) and $x_{CO2,AR}$ (vol%) are the measured concentrations of O_2 and CO_2, respectively, at the outlet of air reactor during fuel operation.

Attrition rate of the oxygen carrier particles is estimated by calculating the loss rate of fines (L_f) that have a size smaller than 63 μm, as seen in Eq. (6). These fines were collected from air-reactor filters, FR chimney and water seal, as stated in Section 2.3.

$$L_f = \frac{\Delta m_{fines}}{\Delta t} \cdot \frac{1}{m_I} \cdot 100\% \quad (6)$$

where the Δm_{fines} (kg) is the mass of fines collected at a time period of Δt (h) with the details of calculation in the *Supporting Information*, and m_I (kg) represents the corresponding oxygen carrier inventory in that period, thus the L_f takes the unit of wt%·h^{-1}.

The lifetime (t_{life}) of the oxygen carrier particles can be easily calculated after knowing the L_f, as shown in the following equation.

$$t_{life} = \frac{100}{L_f} \quad (7)$$

where the t_{life} has a unit of hour, and can be used for estimating the turnover of oxygen carrier bed material.

4. Results and discussion

4.1. Gaseous O_2 release in N_2 environment

The capability of continuously generating gaseous O_2 was examined for fresh and used EB manganese ore particles in the 10 kW_{th} unit. As an example, Fig. 3 shows the fuel-reactor O_2 concentration in N_2 and the air-reactor O_2 concentration under the air fluidisation during a temperature increase to 820 °C as well as at a roughly constant fuel-reactor temperature of 975 °C. In the case of Fig. 3(a), the fuel-reactor bed was initially fluidised by 100% air in the first 53 min with the fuel-reactor temperature being increased from room level to 600 °C. After that, the fluidisation of fuel reactor was switched to 100% N_2, thus a rapid decrease of fuel-reactor O_2 concentration was registered. The small decrease of air-reactor O_2 concentration detected at the same time was caused by the dilution of N_2 from the LS1 shown in Fig. 2. The O_2 concentration of the fuel reactor was close to zero until the fuel-reactor

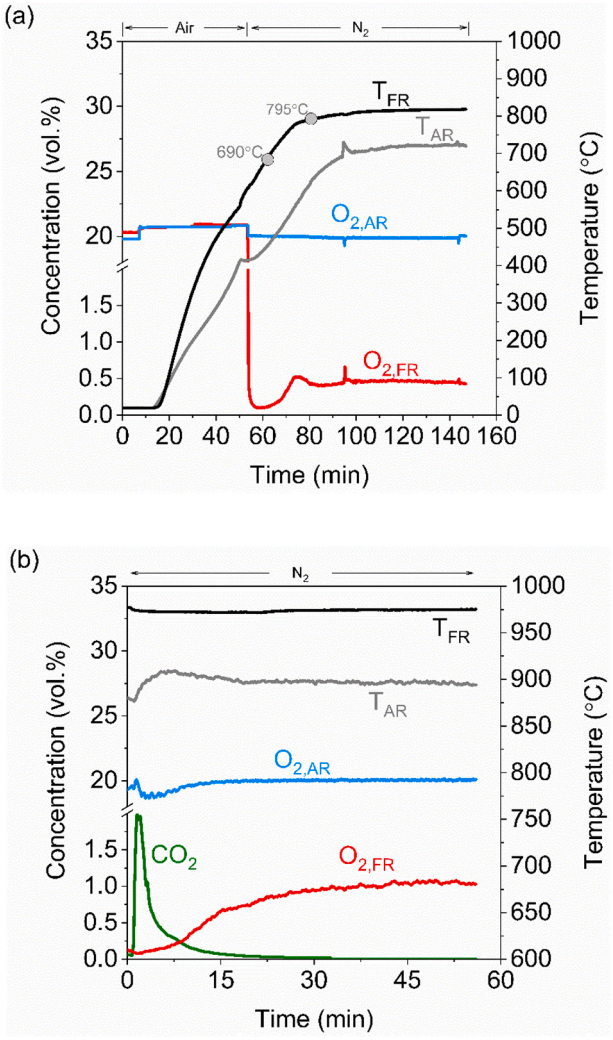

Fig. 3. Release of gaseous O_2 from the EB manganese ore in N_2 atmosphere for (a) fresh-prepared particles under a temperature increase from room level to 820 °C, data from test series 1 and (b) used particles at 975 °C after 42 h of hot operation or 21 h of combustion with different fuels under various operation conditions, data from test series 2.

temperature passed 690 °C, indicating that O_2 release was initiated at this temperature. With further increase of temperature, a continuous growth in O_2 concentration was observed up to 795 °C. A stable O_2 concentration of around 0.45 vol% was maintained to the end of N_2 fluidisation, even though the fuel reactor temperature was further increased to 820 °C. The air reactor has a slower temperature increase than the fuel reactor, and a stable temperature was maintained at around 720 °C. Continuous O_2 release from the fuel reactor bed was maintained for approximately 1 h until this test was terminated.

For the used manganese ore particles, i.e. after 21 h of operation with different fuels, the O_2 release in N_2 environment is shown in Fig. 3(b). After switching to N_2 in Fig. 3(b), a concentration of CO_2 was detected with the peak value at 2.0 vol%, as a result of the combustion of the little residual fuel from the fuel chute, which might be favoured by the gaseous O_2 released from the bed material in the same period. The CO_2 concentration went gradually to close to zero after 15 min of fluidisation with N_2. Meanwhile, the O_2 concentration was gradually increased to a stable value of around 1.0 vol% after around 40 min of fluidisation with N_2. The fuel-reactor temperature was roughly constant at 975 °C, while an initial increase and then a gradual decrease of air-reactor temperature was noticed. This might be caused by the change of fluidisation-gas flow in air reactor to adjust the circulation of oxygen carrier particles.

Comparing Fig. 3(a) and (b), it can be found that the temperature has a positive effect on O_2 concentration, i.e. 0.45 vol% at 820 °C and 1.0 vol % at 975 °C. The concentrations measured may be controlled in part by equilibrium, which means that in presence of a fuel that consumes the oxygen and the release rate could increase [55]. Nevertheless, it is concluded that the feature of gaseous O_2 release from the EB manganese ore is maintained after fuel operations.

In order to maintain high circulation, the flow to the air reactor is much higher than what is needed to supply the oxygen released in the fuel reactor, and consequently the oxygen concentration is very high in the air reactor. It is not unlikely that the high oxygen concentrations in the air reactor enhances the oxygen release somewhat. A laboratory batch test indicated that the release of oxygen was higher after 180 s after a change from 21% oxygen to inert gas, as compared to a to a change from 5% oxygen to inert gas. It can also be noted that the air-reactor temperature is lower than the fuel-reactor temperature, which would normally not be the case. A similar laboratory-reactor test with varied oxidation temperature showed little effect on the oxygen release.

For the tests conducted with fuel below, the oxygen concentrations in the air reactor are lower, but still higher than would be the case of a commercial process. However, the oxygen release is estimated to contribute with a small fraction of the total oxygen transfer. For the dominating normal CLC reaction, the positive effect of higher oxygen concentration and the negative effect of lower air-reactor temperature on kinetics are believed to have a small effect on the outcome. This is because of the oxidation reaction is fast, and the materials circulated to the fuel reactor is expected to be more or less fully oxidised. In laboratory cyclic batch tests, the outgoing concentration of oxygen is typically zero for most of the oxidation reaction [78].

4.2. Reaction progress of different fuels with the oxygen carrier

For fuel operation, the fuel-reactor bed was fluidised with steam, while the flow of N_2 entering from the fuel container and pressure measurement ports was around 30% of the flow used for O_2 release tests shown in Fig. 3. Under these conditions, the dry O_2 concentration in the first 5 min before fuel addition of Fig. 4(a) is around 3 times of that in Fig. 3(a) at the same temperature of 820 °C.

After the start of solid fuels, the O_2 concentration in the fuel reactor dropped rapidly to zero, indicating a part of the fuel was converted via CLOU mode, while the other part was likely burnt under normal CLC mode, i.e. gasification first and then oxidation of gasification products by the oxygen carrier. However, the relative importance of CLOU as compared to CLC mode is not fully known. The temperature in the air reactor increased to a higher level, following fuel addition, which is related to the exothermic oxidation of the reduced oxygen carrier by air [16]. As fuel was continuously fed, some differences in the combustion pattern were observed. In Fig. 4(a), the combustion of BP fuel with the fresh oxygen carrier is shown, and it takes some time for the manganese ore particles to become stable. In this case, a slow increase in CO_2 and a gradual decrease in CO are seen from $t = 10$ min to $t = 38$ min. Stable combustion was achieved after $t = 38$ min with a CO_2 concentration of 35 vol% being reached. Similar concentration of CO and CH_4 was found at around 4 vol%, while a bit lower of H_2 was observed. The combustion of SWC and GWC char shows a similar distribution of CO_2, H_2, CO and CH_4, albeit the main combustion product of SWC and GWC was CO_2 with CO and H_2 as the intermediate gasification products of char. In both cases, the concentrations of CO and H_2 are very close, while little CH_4 was measured because of the low fractions of volatiles in the two fuels. It is also noticed that in the two hours of operation with GWC char in Fig. 4 (c), a slight decrease in CO_2 and slow rising of CO and H_2 are found as a function of time. This can be related to the elutriation of manganese ore particles to the chimney, air-reactor filter and water seal of the system, which led to a gradually decreasing oxygen carrier inventory, thus a slightly slower solids circulation.

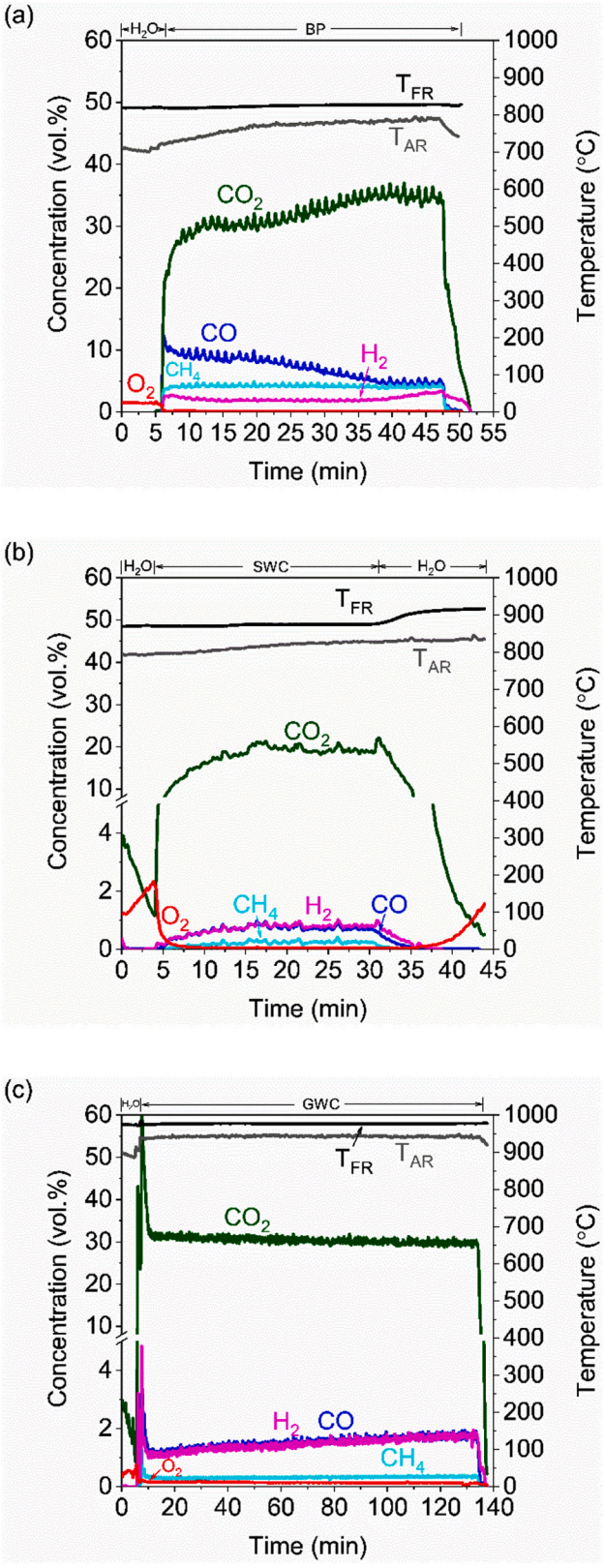

Fig. 4. Typical gas concentration and temperature variation as a function of time for using (a) 6.0 kW_{th} BP pellets at a fuel reactor temperature of around 820 °C, data from test series 3, (b) 1.8 kW_{th} SWC wood char at a fuel reactor temperature of around 875 °C, the fuel reactor temperature increase at around $t = 33$ min is to switch to another operation condition, data from test series 7 and (c) 6.0 kW_{th} GWC wood char at a fuel reactor temperature of around 975 °C, data from test series 10.

4.3. Effect of operation condition

4.3.1. Effect of fuel reactor temperature

Elevation in temperature can promote the oxidation reactions of gases by the oxygen carrier as well as the rate of char gasification due to the faster reaction kinetics [79,81]. Thus, a higher carbon capture was generally attained at a higher temperature for all the fuels, as seen in Fig. 5, which is a result of less char following the oxygen carrier to the air reactor. As the fuel-reactor temperature was increased, combustibles including CH_4, CO and H_2 were lowered while the normalised CO_2 concentration was improved, which led to less oxygen demand. Although similar trends of temperature were observed for the combustion of the three fuels, the degree of fuel conversion varied, especially when comparing the BP and SWC fuels in Fig. 5(a) and (b), respectively. The carbon capture for BP was increased by 2% from 97% at 820 °C to 99% at 975 °C, whereas a great improvement of 28% was achieved for SWC char in the same temperature range. This phenomenon can be ascribed to the different char fractions in the two fuels, which leads to a higher leakage of char to the air reactor for the high-char SWC as compared to the high-volatile BP fuel. Nevertheless, the losses of char to the air reactor can be minimised by using a higher reaction temperature, since the carbon capture at the highest temperature approached 99% for all the three fuels. By comparing the combustibles from BP and the two wood chars it can be seen that more fuel gases remain to be oxidised for the BP, thus a higher oxygen demand of 19.5–29.6% was seen for this fuel, while it can be as low as 2.6% for the SWC wood char. For the two chars, the SWC shows similar values of the normalised CO_2 concentration as well as oxygen demand and content of combustibles as compared to GWC at the same temperatures. The difference in oxygen demand for BP and the two chars is mainly attributed to the different volatile contents for the three fuels. Char can mix with the bed material and, during gasification, release gases in close contact with the oxygen carrier bed material. The volatiles, on the other hand, may go into the dilute phase, bubble phase, and bypass the bed material, leading to a higher oxygen demand. Therefore, it is important to provide fluidisation conditions giving good contact between volatiles released and bed material.

4.3.2. Effect of circulation index

The circulation of oxygen carrier transports the oxidised particles to the fuel reactor and the reduced particles to the air reactor and entrains unconverted char to the air reactor. At a higher circulation index, a higher availability of oxygen can be realised because more oxidised oxygen carrier is transferred to the fuel reactor. Thus, more effective combustion can be reached, leading to lower normalised concentration of CO, CH_4 and H_2 as seen in Fig. 6(a) and (b) at a higher CI. The better oxidation of these combustibles resulted in lower oxygen demand and higher normalised CO_2 concentration. At the similar CI, the SWC char shows a lower oxygen demand as compared to BP fuel, which is related to the fractions of volatiles in these fuels. The volatiles can be partially enclosed in the rising bubbles and bypass the bed material without reacting with the oxygen carrier, thus the more-volatile-containing BP can result in more unconverted components than the less-volatile-containing SWC char at the outlet of fuel reactor. As said, circulation can also entrain char from the fuel reactor to the air reactor, which occurred for SWC as the circulation index was increased, see Fig. 6(b). A decrease of around 1.5% in carbon capture is seen as the circulation index was increased to higher than 600 kPa·(L_N·min^{-1}) in Fig. 6(b), which led to some CO_2 being detected in the air reactor, not shown here. On the contrary, the influence of CI on the carbon capture for BP is not so significant, due to the low char content in this fuel. Nevertheless, the carbon capture can be improved by implementing a carbon stripper between the fuel and air reactor [43,82], which can recirculate the entrained char back to the fuel reactor for further conversion.

4.3.3. Effect of fuel power

The different combustion behaviours under various fuel powers can

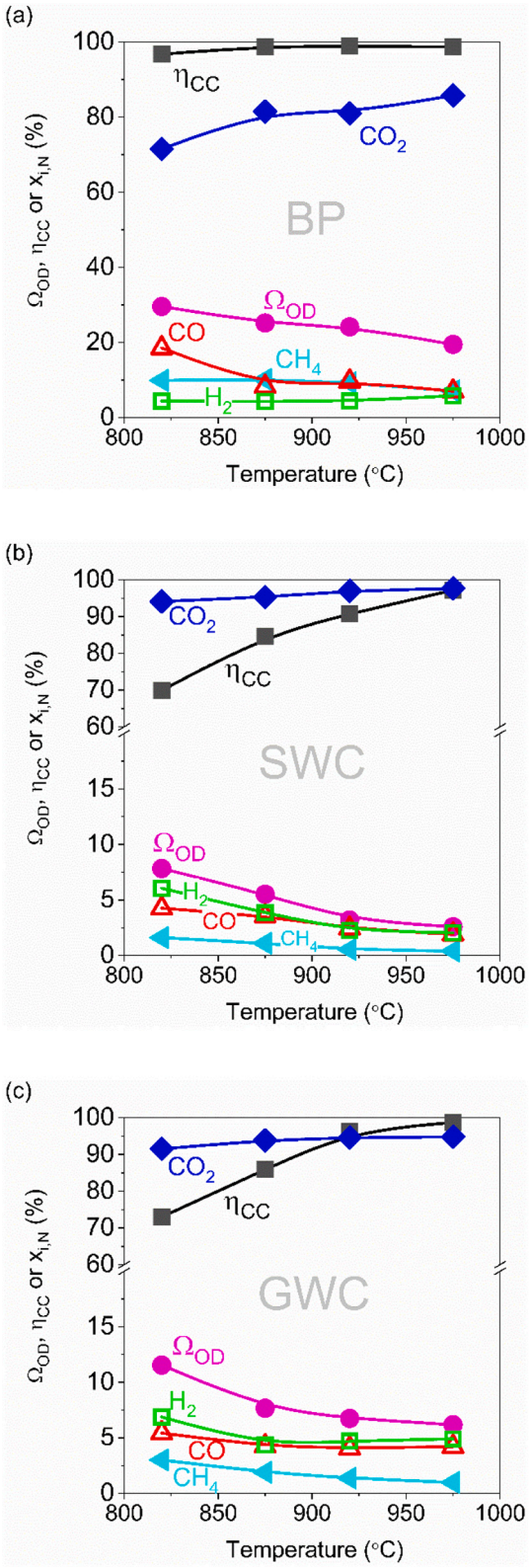

Fig. 5. Variation of oxygen demand (Ω_{OD}), carbon capture (η_{CC}) and normalised gas concentration ($x_{i,N}$) of CH_4, CO, CO_2 and H_2 as a function of fuel-reactor temperature for using (a) BP fuel with CI ≈ 100 kPa·(L_N·min^{-1}), data from test series 3, (b) SWC char with CI ≈ 200 kPa·(L_N·min^{-1}), data from test series 7 and (c) GWC char with CI ≈ 200 kPa·(L_N·min^{-1}), data from test series 10. Note the breaks of Y-axis in (b) and (c) panels.

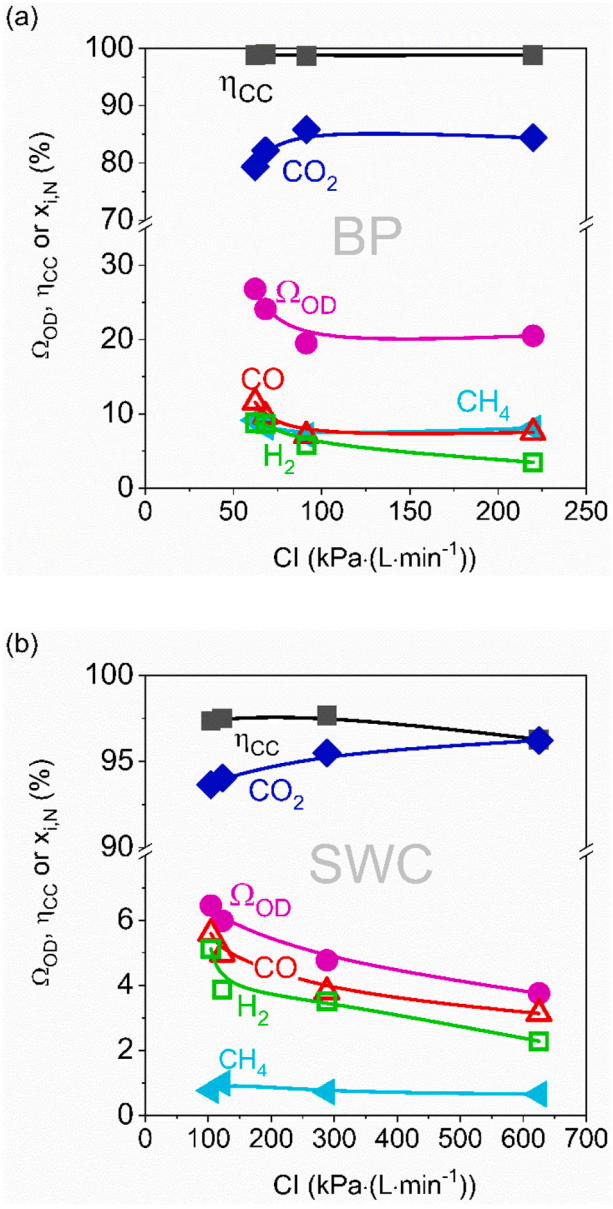

Fig. 6. Variation of oxygen demand (Ω_{OD}), carbon capture (η_{CC}) and normalised concentration ($x_{i,N}$) of CH_4, CO, CO_2 and H_2 as a function of circulation index (CI) for using (a) BP at a fuel-reactor temperature of 975 °C, data from test series 3 and (b) SWC at a fuel-reactor temperature of 985 °C, data from test series 6. Note the different scales and the break in Y-axis.

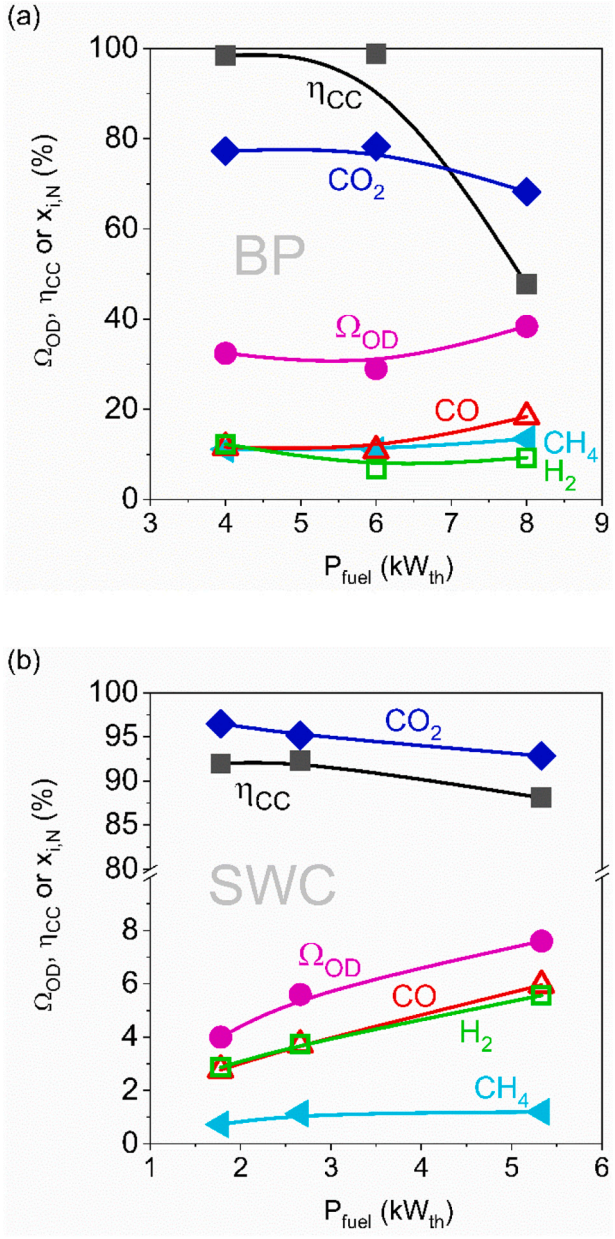

Fig. 7. Variation of oxygen demand (Ω_{OD}), carbon capture (η_{CC}) and normalised concentration ($x_{i,N}$) of CH_4, CO, CO_2 and H_2 as a function of thermal power (P_{fuel}) for using (a) BP fuel with CI ≈ 80 kPa·(L_N·min^{-1}), data from test series 3, 4 and 5, and (b) SWC fuel with CI ≈ 200 kPa·(L_N·min^{-1}), data from test series 7, 8 and 9. The fuel-reactor temperature was 920 °C. Note the breaks in the Y-axis of the (b) panel.

be seen in Fig. 7 using BP and SWC fuels. For the BP fuel in Fig. 7(a), an increase of fuel power from 4 to 6 kW_{th} gives no big changes of carbon capture, oxygen demand or the normalised gas concentration, which could suggest that the oxidative capacity of the manganese ore is sufficient for such fuel throughputs under this operating condition. However, as the fuel power was increased to 8 kW_{th}, significantly lower carbon capture and normalised CO_2 concentration were observed, while the fractions of combustibles were higher. Using the SWC fuel, a similar effect of fuel power was also noticed, as seen in Fig. 7(b). In this case, the char gasification rate has higher importance, due to the high fraction of char in the SWC fuel. This could explain the low fraction of CH_4 at the outlet of fuel reactor, i.e. only around 1%. As the fuel power is raised, the carbon capture falls from 92% at 1.8 kW_{th} to 88% at 5.3 kW_{th}. Meanwhile, the fractions of combustibles also increased at higher fuel power, which resulted in a lower normalised CO_2 concentration and a higher oxygen demand at the outlet of fuel reactor.

4.4. Reactivity of the manganese ore

The reactivity of the manganese ore is checked by comparing with the ilmenite in terms of normalised concentration of combustibles and the oxygen demand for BP and SWC fuels, as seen in Fig. 8. Using the BP fuel and EB manganese ore, the normalised concentrations of CH_4, CO and H_2 were varying at around 8.3%, 8.1% and 3.9%, respectively, which resulted in an oxygen demand of 20.4–22.4%, as seen in Fig. 8(a). This is different compared to ilmenite under similar operation conditions. In the case of ilmenite, much more CO and H_2 as well as slightly more CH_4 were found in the gas stream leaving the fuel reactor. The average normalised concentration of CH_4, CO and H_2 for ilmenite were 1.1, 2.4 and 2.0 times the corresponding values for the manganese ore, which led to a higher oxygen demand of around 30%. A lower fraction of

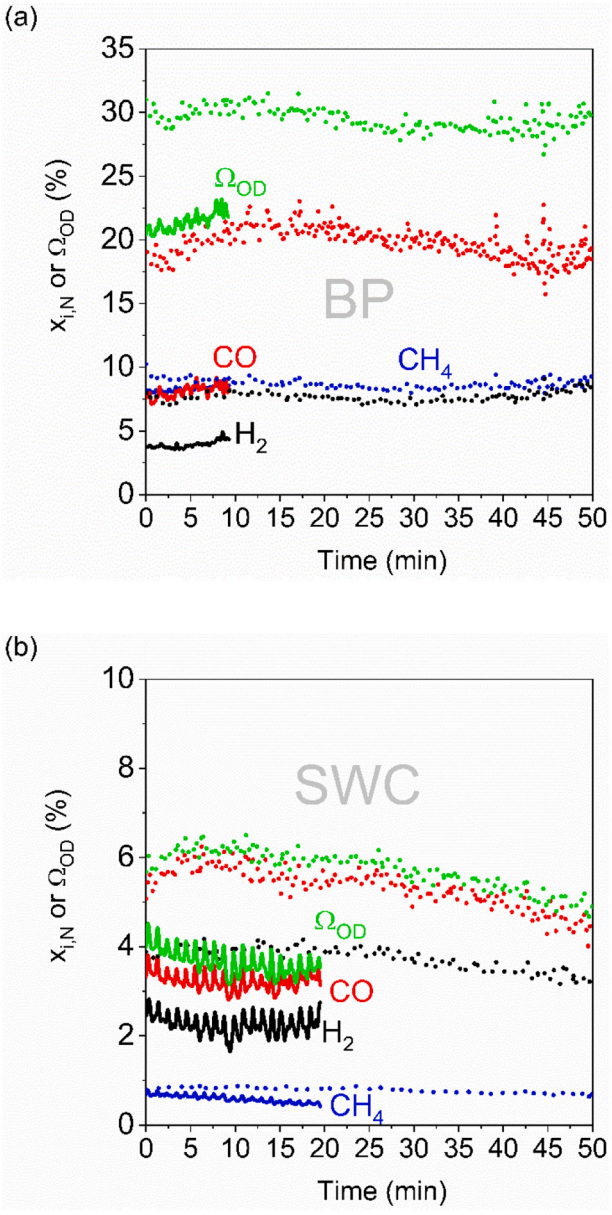

Fig. 8. Comparison of the EB manganese ore (continuous lines) and ilmenite (dot lines) in terms of the normalised gas concentration $x_{i,N}$ for CH_4, CO and H_2 and the oxygen demand Ω_{OD} using (a) 6 kW_{th} BP at a fuel-reactor temperature of 975 °C with CI ≈ 200 kPa·(L_N·min^{-1}), data from test series 3 and 15, and (b) 6 kW_{th} SWC at a fuel-reactor temperature of 985 °C with CI ≈ 350 kPa·(L_N·min^{-1}), data from test series 6 and 16.

combustibles in the case of manganese ore than ilmenite was also found with the use of SWC char in Fig. 8(b). Because similar operation conditions were used, it can be concluded that the manganese ore shows a higher reactivity than the ilmenite.

The dominant reason for the better fuel conversion compared to the ilmenite is not fully known for this specific EB manganese ore, however, some potential explanations are discussed as follows. Higher reactivity could be a result of the release of gaseous O_2 from this manganese ore, as discussed in Section *4.1*. In this case, a part of fuel can be oxidised by the gaseous O_2, i.e. under CLOU mode [18,22]. Another explanation could be the higher gas-solid reactivity of manganese ore than for the ilmenite during their interactions with the fuel gases, which was noticed for other manganese ores in previous works [33,52,53]. Noting the higher content of K and Na in the manganese ore, the catalytic effects of alkali elements on the char gasification could also be a potential mechanism. Using other manganese ores, the presence of K and Na was reported to lead to a faster char gasification, which finally resulted in a better conversion of solid fuels [32,59]. However, the impact of alkali in the oxygen carrier is likely less for biomass fuels that normally have a higher alkali content.

4.5. Attrition rate of the manganese ore

4.5.1. Distribution of fines in different parts of the system

During the operation of the 10 kW_{th} unit, particles from the air-reactor filter, fuel-reactor chimney and the water seal were regularly collected, dried and subjected to particle size distribution analysis using a series of standard test sieves. The fuel-reactor chimney and water seal particles were collected during cleaning periods while fuel was stopped. In the case of air-reactor filter particles, the two filters can be intermittently switched during operation which facilitates sampling. Therefore, more samples were collected from the air-reactor filter. In some cases, char was found in the particles from the fuel reactor chimney and water seal, of which the weight fraction of char was determined by heat treatment at a high temperature in air atmosphere. Details of the testing procedure for particle size distribution of the 35 samples and the heat treatment of fines are given in the *Supporting Information* of this work. Accordingly, the weight fraction for particles smaller than 63 μm is displayed as a function of hot operation hours in Fig. 9. During the first hours of operation, around 48 wt% of the oxygen carrier particles from the air-reactor filter consisted of fine material. After 9 h of hot operation, the weight proportion went down and took a value in the interval of 10-24 wt%. Apart from the air-reactor filter, the percentage of fines from fuel-reactor chimney and water seal particles also varied in the range of 2-14 wt% and 0.6–7.5 wt%, respectively. It is evident that the particles from the air-reactor filter have a higher fraction of fines, which can be a result of the separation by the cyclone connecting to the riser of the air reactor, as seen in Fig. 2. The mass of fines produced is calculated using the amounts of particles collected in a time period, see *Supporting Information*, and is used to estimate the attrition rate of the manganese ore in the following section.

4.5.2. Attrition rate

In addition to the weight of fines collected, the total oxygen carrier inventory inside the reactor in the same period must be known, which was calculated by closely monitoring the amounts of particles introduced and extracted from the system. As fuel addition has shown an increased oxygen carrier attrition compared to operations without fuel

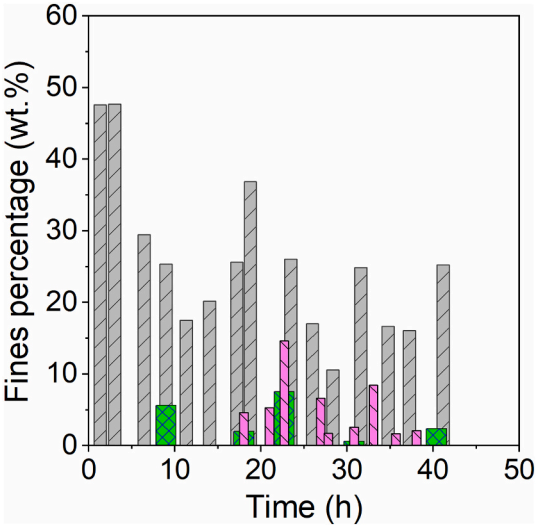

Fig. 9. Weight fraction of fines (d_p < 63 μm) as a function of hot operation time for different parts (air-reactor filter: ■, fuel-reactor chimney: ■ and water seal: ■) of the 10 kW_{th} unit.

[62], two cases have been considered for the estimation of attrition rate: (*i*) hot conditions at an air reactor temperature higher than 500 °C and (*ii*) fuel operation, i.e. excluding the time without fuel from the hot conditions. If chemical transformation is the key mechanism leading to attrition, fuel operation time would be the most relevant measure, but if the attrition is only mechanical the total time of operation would be more relevant. Most likely attrition also occurs in absence of fuel, so the most valid value of attrition is between these two. Normally, operation time with fuel is used for lifetime estimations, which is then a conservative approach. These two cases are presented in Fig. 10, where the attrition rate decreases as a function of time for hot or fuel operation. In the first 10 h of fuel operation, a higher attrition rate was observed. However, after 25 h of hot operation or 10 h of fuel combustion, the attrition rate was reduced to a relatively stable value of 0.27 and 0.12 wt %/h for fuel and hot operation, respectively. Accordingly, the lifetime of the manganese ore particles is estimated at 370–830 h, which is in a comparable level as that for ilmenite determined in a 100 kW_{th} unit, i.e. 700–800 h [83] and somewhat higher than the other manganese ores reported in previous works, i.e. 100–400 h [61,62]. Thus, the lifetime of EB manganese ore might be suitable for a large-scale CLC system [73].

5. Morphology of the manganese ore

The fresh EB particles, i.e. before any operation, and the used particles after the entire campaign and the air-reactor filter particles from test series 14 were subject for morphology analysis with the light microscope, as seen in Fig. 11. Some typical particles were further used for size and edge angle measurement, based on an external calibration of the microscope, to have a preliminary comparison. As seen in Fig. 11(a), the fresh oxygen carrier particles have a wide range of irregular shapes and sharp edges with typical angles at around 47–73°. Some big particles can have a length of 1.1 mm, while the small particles can be lower than 0.1 mm, however, their narrowest section is smaller than or equal to 0.5 mm as a result of sieving with this same size of mesh. The shining spots on the particles are a result of reflection of light by the metal components in the ore. Minor amount of fines are observed among the fresh particles, which have escaped the wet sieving process dedusting the oxygen carrier. After the use with all the fuels and hot operations, the particles became rounder, as a result of the rounding effect in the fluidised bed, although some particles still have edge angles of 71–76°, as seen in Fig. 11(b). The rounding effect in the reactor could be a partial reason of fines generation. Further, some smaller particles, shown in yellowish circles in Fig. 11(b), tend to stick together to form small

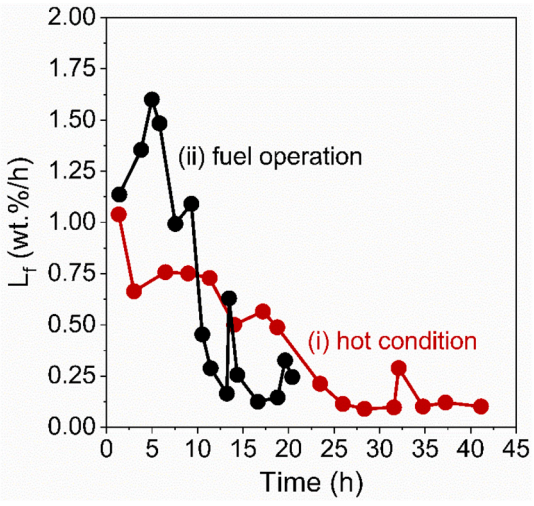

Fig. 10. Estimated attrition rate of the EB manganese ore particles as a function of operation time considering (i) hot condition (●) as the air reactor temperature was higher than 500 °C or (ii) only during fuel operation (●).

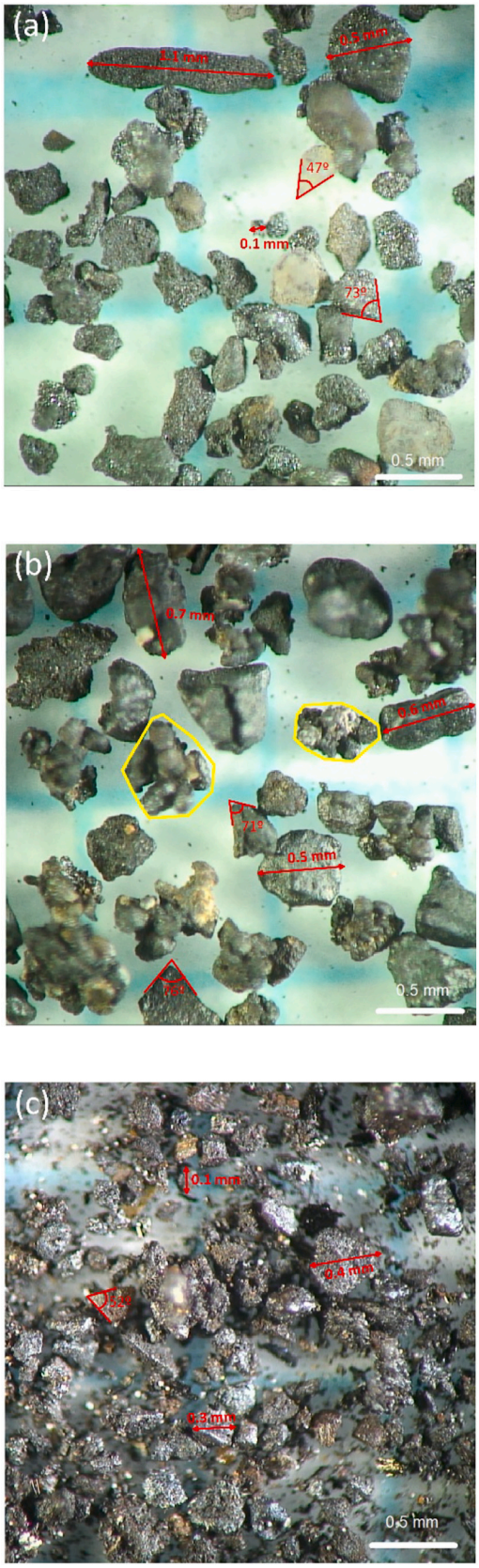

Fig. 11. Light microscope images of (a) fresh prepared EB particles, (b) used EB particles after all the 14 series of tests and (c) particles collected from air-reactor filter during series 14 operation.

blocks. However, there is no interaction among the other bigger particles. Nevertheless, the fluidisation was maintained well during the entire campaign, and no hard agglomerations occurred. In the case of air-reactor filter particles, much lower size and more fragments are seen in Fig. 11(c). The maximum size of particles is measured as 0.1–0.4 mm, while others are much smaller than 0.1 mm that cannot be well identified and measured by this microscope. These fines represent the main loss of material from the system, which has already been demonstrated in Fig. 9 and the *Supporting Information* of this work.

6. Conclusions

Using a new manganese ore, a series of experimental tests were carried out in a recently commissioned 10 kW_{th} unit with different biomass-based solid fuels. The manganese ore has the capability of continuously releasing gas-phase O_2 in N_2 environment, i.e. CLOU behaviour, at concentrations of 0.45–1.0 vol%. However, the contribution of gaseous O_2 release on solid fuel combustion cannot be identified from this work. In CLC tests with solid fuels, fuel-reactor temperature and solids circulation generally have positive effects on the combustion performance, but a too high circulation could decrease the carbon capture efficiency, while the fuel power input also showed some effects. The oxygen demand varied in the range of 2.6–38.4%, where the lowest oxygen demand was achieved at 975 °C for the combustion of a Swedish wood char. The new manganese ore showed higher reactivity than the often-used ilmenite. Thus, the oxygen demand was decreased by 8–10% using the manganese ore. In the entire campaign of tests, there was no defluidisation of the manganese ore oxygen carrier. The attrition rate of the manganese ore particles decreased as a function of time of operation, and finally approached a relatively stable value. The estimated lifetime of the manganese ore particles is 370–830 h, which is at a comparable level as ilmenite.

Nomenclatures

AR	air reactor
BECCS	biomass energy with carbon capture and storage
Bio-CLC	biofuel chemical looping combustion
CCS	carbon capture and storage
CI	circulation index, $kPa \cdot (L_N \cdot min^{-1})$
CLC	chemical looping combustion
CLOU	chemical looping with oxygen uncoupling
$F_{AR,out}$	volumetric flow of gas leaving the air reactor, $L_N \cdot min^{-1}$
FR	fuel reactor
ICP-SFMS	inductively coupled plasma sector field mass spectrometry
L_f	loss rate of fines, $wt\% \cdot h^{-1}$
LHV	lower heating value of fuel, $MJ \cdot kg^{-1}$
LS1	lower position loop seal
LS2	higher position loop seal
m_I	oxygen carrier inventory in the system, kg
MeO_x	oxygen carrier in oxidation state
$MeO_{x\text{-}1}$	oxygen carrier in reduced state
P_{fuel}	fuel thermal power input, kW_{th}
t	time, min
t_{life}	lifetime of the oxygen carrier particles, h
T_{AR}	air reactor temperature, °C
T_{FR}	fuel reactor temperature, °C
$x_{i,AR}$	measured concentration of component i (i = CO, CO_2 or O_2) from the air reactor
$x_{i,FR}$	measured concentration of component i (i = CO, CH_4, H_2 or CO_2) from the fuel reactor
$x_{i,N}$	normalised concentration of component i (i = CO, CH_4, H_2 or CO_2) from the fuel reactor
$x_{O2,ini}$	initial O_2 concentration at the outlet of air reactor before fuel operation
Δm_{fines}	mass of fines collected, kg
ΔP_{riser}	measured pressure drop over the riser of air reactor, kPa
Δt	time period for collecting the fines, h
Φ_0	stoichiometric O_2 moles per mole C for full combustion of fuel
Ω_{OD}	oxygen demand for full combustion at the fuel reactor exit
η_{CC}	carbon capture efficiency
$\dot{m}_{fuel}$	mass flow rate of fuel entering the system, $kg \cdot s^{-1}$

Declaration of Competing Interest

None.

Acknowledgements

This work was carried out as part of the OxyCar-FBC project, which is conducted within the framework of ERA-NET Bioenergy and funded by the Swedish Energy Agency (P43936-1).

Appendix A. Supplementary data

Supplementary data to this article can be found online at https://doi.org/10.1016/j.fuproc.2021.106743.

References

[1] R.K. Pachauri, M.R. Allen, V.R. Barros, J. Broome, W. Cramer, R. Christ, et al., Climate Change 2014: Synthesis Report. Contribution of Working Groups I, II and III to the Fifth Assessment Report of the Intergovernmental Panel on Climate Change, IPCC, Geneva, Switzerland, 2014.
[2] NOAA-ESRL, Trends in Atmospheric Carbon Dioxide: Annual Mean Growth Rate for Mauna Loa, Hawaii. https://www.esrl.noaa.gov/gmd/ccgg/trends/, 2020 accessed 15 October 2020.
[3] V. Masson-Delmotte, P. Zhai, H.-O. Pörtner, D. Roberts, J. Skea, P.R. Shukla, et al., Global Warming of 1.5°C. An IPCC Special Report on the Impacts of Global Warming of 1.5°C above Pre-industrial Levels and Related Global Greenhouse Gas Emission Pathways, in the Context of Strengthening the Global Response to the Threat of Climate Change, Sustainable Development, and Efforts to Eradicate Poverty, IPCC, 2018.
[4] International Energy Agency (IEA), Energy Technology Perspectives 2017, OECD/IEA, Paris, 2017.
[5] United Nations Framework Convention on Climate Change (UNFCCC), The Paris Agreement, Paris, 2015.
[6] W.K. Lewis, E.R. Gilliland, Production of Pure Carbon Dioxide, US Patent 2665972A, 1954.
[7] M. Ishida, H. Jin, A new advanced power-generation system using chemical-looping combustion, Energy 19 (1994) 415–422.
[8] A. Lyngfelt, Chemical Looping Combustion: Status and Development challenges, Energy Fuel 34 (2020) 9077–9093.
[9] H. Zhao, X. Tian, J. Ma, M. Su, B. Wang, D. Mei, Development of tailor-made oxygen carriers and reactors for chemical looping processes at Huazhong University of Science & Technology, Int. J. Greenhouse Gas Control 93 (2020), 102898.
[10] H. Zhao, X. Tian, J. Ma, X. Chen, M. Su, C. Zheng, Y. Wang, Chemical looping combustion of coal in China: comprehensive progress, remaining challenges, and potential Opportunities, Energy Fuel 34 (2020) 6696–6734.
[11] A. Lyngfelt, B. Leckner, Technologies for CO_2 separation, in: Minisymposium on Carbon Dioxide Capture and Storage, Göteborg, Sweden, 1999.
[12] M.M. Hossain, H.I. de Lasa, Chemical-looping combustion (CLC) for inherent CO_2 separations-a review, Chem. Eng. Sci. 63 (2008) 4433–4451.
[13] A. Lyngfelt, M. Johansson, T. Mattisson, Chemical-looping combustion-status of development, in: 9th International Conference on Circulating Fluidized Beds, 2008. Hamburg, Germany.
[14] J. Adánez, A. Abad, F. García-Labiano, P. Gayán, L.F. de Diego, Progress in Chemical-Looping Combustion and Reforming technologies, Prog. Energy Combust. Sci. 38 (2012) 215–282.
[15] Q. Imtiaz, D. Hosseini, C.R. Müller, Review of Oxygen carriers for chemical looping with oxygen uncoupling (CLOU): thermodynamics, material development, and synthesis, Energy Technol. 1 (2013) 633–647.
[16] E. Jerndal, T. Mattisson, A. Lyngfelt, Thermal analysis of chemical-looping combustion, Chem. Eng. Res. Des. 84 (2006) 795–806.
[17] D. Karami, A.H. Soleimanisalim, M.H. Sedghkerdar, N. Mahinpey, Preparation of Novel Oxygen Carriers Supported by Ti, Zr-Shelled γ-Alumina for Chemical Looping Combustion of methane, Ind. Eng. Chem. Res. 59 (2020) 3221–3228.
[18] D. Mei, A. Abad, H. Zhao, J. Adánez, Characterization of a sol–gel derived CuO/$CuAl_2O_4$ oxygen carrier for chemical looping combustion (CLC) of gaseous fuels: Relevance of gas–solid and oxygen uncoupling reactions, Fuel Process. Technol. 133 (2015) 210–219.
[19] T. Mattisson, A. Lyngfelt, H. Leion, Chemical-looping with oxygen uncoupling for combustion of solid fuels, Int. J. Greenhouse Gas Control 3 (2009) 11–19.

[20] T. Mattisson, Materials for chemical-looping with oxygen uncoupling, ISRN Chem. Eng. 526375 (2013).
[21] I. Adánez-Rubio, A. Abad, P. Gayán, L.F. de Diego, F. García-Labiano, J. Adánez, Identification of operational regions in the Chemical-Looping with Oxygen Uncoupling (CLOU) process with a Cu-based oxygen carrier, Fuel 102 (2012) 634–645.
[22] T. Mendiara, I. Adánez-Rubio, P. Gayán, A. Abad, L.F. de Diego, F. García-Labiano, J. Adánez, Process Comparison for Biomass Combustion: in Situ Gasification-Chemical Looping Combustion (iG-CLC) versus Chemical Looping with Oxygen Uncoupling (CLOU), Energy Technol. 4 (2016) 1130–1136.
[23] M. Rydén, A. Lyngfelt, Ø. Langørgen, Y. Larring, A. Brink, S. Teir, H. Havåg, P. Karmhagen, Negative CO_2 Emissions with Chemical-Looping Combustion of Biomass – a Nordic Energy Research Flagship Project, Energy Procedia 114 (2017) 6074–6082.
[24] T. Mendiara, F. García-Labiano, A. Abad, P. Gayán, L.F. de Diego, M.T. Izquierdo, J. Adánez, Negative CO_2 emissions through the use of biofuels in chemical looping technology: a review, Appl. Energy 232 (2018) 657–684.
[25] A. Lyngfelt, Chemical-looping combustion of solid fuels – Status of development, Appl. Energy 113 (2014) 1869–1873.
[26] T. Mattisson, M. Keller, C. Linderholm, P. Moldenhauer, M. Rydén, H. Leion, A. Lyngfelt, Chemical-looping technologies using circulating fluidized bed systems: Status of development, Fuel Process. Technol. 172 (2018) 1–12.
[27] J. Adánez, A. Abad, T. Mendiara, P. Gayán, L.F. de Diego, F. García-Labiano, Chemical looping combustion of solid fuels, Prog. Energy Combust. Sci. 65 (2018) 6–66.
[28] M. Matzen, J. Pinkerton, X. Wang, Y. Demirel, Use of natural ores as oxygen carriers in chemical looping combustion: a review, Int. J. Greenhouse Gas Control 65 (2017) 1–14.
[29] T. Mendiara, R. Pérez, A. Abad, L.F. de Diego, F. García-Labiano, P. Gayán, J. Adánez, Low-cost Fe-based oxygen carrier materials for the iG-CLC process with coal, Ind. Eng. Chem. Res. 51 (2012) 16216–16229.
[30] Y. Wang, X. Tian, H. Zhao, K. Liu, The use of a low-cost oxygen carrier prepared from red mud and copper ore for in situ gasification chemical looping combustion of coal, Fuel Process. Technol. 205 (2020) 106460.
[31] T. Song, L. Shen, Review of reactor for chemical looping combustion of solid fuels, Int. J. Greenhouse Gas Control 76 (2018) 92–110.
[32] D. Mei, T. Mendiara, A. Abad, L.F. de Diego, F. García-Labiano, P. Gayán, J. Adánez, H. Zhao, Manganese Minerals as Oxygen Carriers for Chemical Looping Combustion of coal, Ind. Eng. Chem. Res. 55 (2016) 6539–6546.
[33] D. Mei, T. Mendiara, A. Abad, L.F. de Diego, F. García-Labiano, P. Gayán, J. Adánez, H. Zhao, Evaluation of Manganese Minerals for Chemical Looping Combustion, Energy Fuel 29 (2015) 6605–6615.
[34] M. Arjmand, H. Leion, T. Mattisson, A. Lyngfelt, Investigation of different manganese ores as oxygen carriers in chemical-looping combustion (CLC) for solid fuels, Appl. Energy 113 (2014) 1883–1894.
[35] L. Shen, M. Zheng, J. Xiao, R. Xiao, A mechanistic investigation of a calcium-based oxygen carrier for chemical looping combustion, Combust. Flame 154 (2008) 489–506.
[36] A. Abad, M. de las Obras-Loscertales, F. García-Labiano, L.F. de Diego, P. Gayán, J. Adánez, In situ gasification Chemical-Looping Combustion of coal using limestone as oxygen carrier precursor and sulphur sorbent, Chem. Eng. J. 310 (2017) 226–239.
[37] M. Zheng, Y. Xing, K. Li, S. Zhong, H. Wang, B. Zhao, Enhanced Performance of Chemical Looping Combustion of CO with $CaSO_4$-CaO Oxygen carrier, Energy Fuel 31 (2017) 5255–5265.
[38] A. Lyngfelt, B. Leckner, SO_2 capture fluidised-bed boilers: re-emission of SO_2 due to reduction of $CaSO_4$, Chem. Eng. Sci. 44 (1989) 207–213.
[39] T. Pikkarainen, I. Hiltunen, Chemical looping combustion of solid biomass – performance of ilmenite and braunite as oxygen carrier materials, in: European Biomass Conference & Exhibition, Stockholm, Sweden, 2017.
[40] A. Pérez-Astray, T. Mendiara, L.F. de Diego, A. Abad, F. García-Labiano, M. T. Izquierdo, J. Adánez, Improving the oxygen demand in biomass CLC using manganese ores, Fuel. 274 (2020) 117803.
[41] A. Abad, P. Gayán, T. Mendiara, J.A. Bueno, F. García-Labiano, L.F. de Diego, J. Adánez, Assessment of the improvement of chemical looping combustion of coal by using a manganese ore as oxygen carrier, Fuel Process. Technol. 176 (2018) 107–118.
[42] M. Schmitz, C. Linderholm, Chemical looping combustion of biomass in 10- and 100-kW pilots – Analysis of conversion and lifetime using a sintered manganese ore, Fuel 231 (2018) 73–84.
[43] D. Mei, C. Linderholm, A. Lyngfelt, Performance of an oxy-polishing step in the 100 kW_{th} chemical looping combustion prototype, Chem. Eng. J. 409 (2021), 128202.
[44] A. Hedayati, A.H. Soleimanisalim, C. Linderholm, T. Mattisson, A. Lyngfelt, Experimental evaluation of manganese ores for chemical looping gasification in a circulating fluidized bed reactor, submitted for publication, 2020.
[45] S. Yin, L. Shen, M. Dosta, E.-U. Hartge, S. Heinrich, P. Lu, J. Werther, T. Song, Chemical Looping Gasification of a Biomass Pellet with a Manganese Ore as an Oxygen carrier in the Fluidized Bed, Energy Fuel 32 (2018) 11674–11682.
[46] G. Azimi, M. Rydén, H. Leion, T. Mattisson, A. Lyngfelt, $(MnzFe_{1-z})_yO_x$ combined oxides as oxygen carrier for chemical-looping with oxygen uncoupling, AICHE J. 59 (2013) 582–588.
[47] A. Shulman, E. Cleverstam, T. Mattisson, A. Lyngfelt, Manganese/iron, manganese/nickel, and manganese/silicon oxides used in chemical-looping with oxygen uncoupling (CLOU) for combustion of methane, Energy Fuel 23 (2009) 5269–5275.
[48] M. Rydén, H. Leion, T. Mattisson, A. Lyngfelt, Combined oxides as oxygen-carrier material for chemical-looping with oxygen uncoupling, Appl. Energy 113 (2014) 1924–1932.
[49] M. Rydén, A. Lyngfelt, T. Mattisson, Combined manganese/iron oxides as oxygen carrier for chemical looping combustion with oxygen uncoupling (CLOU) in a circulating fluidized bed reactor system, Energy Procedia 4 (2011) 341–348.
[50] S. Sundqvist, M. Arjmand, T. Mattisson, H. Leion, M. Rydén, A. Lyngfelt, Screening of different manganese ores for chemical-looping combustion (CLC) and chemical looping with oxygen uncoupling (CLOU), in: 11th International Conference on Fluidized Bed technology, Beijing, China, 2014.
[51] P. Moldenhauer, A. Serrano, F. García-Labiano, L.F. de Diego, M. Biermann, T. Mattisson, A. Lyngfelt, Chemical-looping combustion of kerosene and gaseous fuels with a natural and a manufactured Mn–Fe-based oxygen carrier, Energy Fuel 32 (2018) 8803–8816.
[52] S. Sundqvist, M. Arjmand, T. Mattisson, M. Rydén, A. Lyngfelt, Screening of different manganese ores for chemical-looping combustion (CLC) and chemical-looping with oxygen uncoupling (CLOU), Int. J. Greenhouse Gas Control 43 (2015) 179–188.
[53] S. Sundqvist, N. Khalilian, H. Leion, T. Mattisson, A. Lyngfelt, Manganese ores as oxygen carriers for chemical-looping combustion (CLC) and chemical-looping with oxygen uncoupling (CLOU), J. Environ. Chem. Eng. 5 (2017) 2552–2563.
[54] I. Adánez-Rubio, P. Gayán, A. Abad, F. García-Labiano, L.F. de Diego, J. Adánez, Kinetic analysis of a Cu-based oxygen carrier: relevance of temperature and oxygen partial pressure on reduction and oxidation reactions rates in Chemical Looping with Oxygen Uncoupling (CLOU), Chem. Eng. J. 256 (2014) 69–84.
[55] S. Sundqvist, T. Mattisson, H. Leion, A. Lyngfelt, Oxygen release from manganese ores relevant for chemical looping with oxygen uncoupling conditions, Fuel 232 (2018) 693–703.
[56] N.M. Pour, G. Azimi, H. Leion, M. Rydén, A. Lyngfelt, Production and examination of oxygen-carrier materials based on manganese ores and $Ca(OH)_2$ in chemical looping with oxygen uncoupling, AICHE J. 60 (2014) 645–656.
[57] P. Frohn, M. Arjmand, G. Azimi, H. Leion, T. Mattisson, A. Lyngfelt, On the high-gasification rate of Brazilian manganese ore in chemical-looping combustion (CLC) for solid fuels, AICHE J. 59 (2013) 4346–4354.
[58] M. Arjmand, H. Leion, A. Lyngfelt, T. Mattisson, Use of manganese ore in chemical-looping combustion (CLC)—effect on steam gasification, Int. J. Greenhouse Gas Control 8 (2012) 56–60.
[59] M. Keller, H. Leion, T. Mattisson, Mechanisms of solid fuel conversion by chemical-looping combustion (CLC) using manganese ore: catalytic gasification by potassium compounds, Energy Technol. 1 (2013) 273–282.
[60] C. Linderholm, A. Lyngfelt, A. Cuadrat, E. Jerndal, Chemical-looping combustion of solid fuels – operation in a 10kW unit with two fuels, above-bed and in-bed fuel feed and two oxygen carriers, manganese ore and ilmenite, Fuel 102 (2012) 808–822.
[61] M. Schmitz, C. Linderholm, P. Hallberg, S. Sundqvist, A. Lyngfelt, Chemical-looping combustion of solid fuels using manganese ores as oxygen carriers, Energy Fuel 30 (2016) 1204–1216.
[62] C. Linderholm, M. Schmitz, M. Biermann, M. Hanning, A. Lyngfelt, Chemical-looping combustion of solid fuel in a 100kW unit using sintered manganese ore as oxygen carrier, Int. J. Greenhouse Gas Control 65 (2017) 170–181.
[63] P. Moldenhauer, S. Sundqvist, T. Mattisson, C. Linderholm, Chemical-looping combustion of synthetic biomass-volatiles with manganese-ore oxygen carriers, Int. J. Greenhouse Gas Control 71 (2018) 239–252.
[64] L. Xu, H. Sun, Z. Li, N. Cai, Experimental study of copper modified manganese ores as oxygen carriers in a dual fluidized bed reactor, Appl. Energy 162 (2016) 940–947.
[65] I. Gogolev, A.H. Soleimanisalim, C. Linderholm, A. Lyngfelt, Commissioning, performance benchmarking, and investigation of alkali emissions in a 10 kW_{th} solid fuel chemical looping combustion pilot, Fuel. 119530 (2020).
[66] T. Berdugo Vilches, F. Lind, M. Rydén, H. Thunman, Experience of more than 1000h of operation with oxygen carriers and solid biomass at large scale, Appl. Energy 190 (2017) 1174–1183.
[67] P. Markström, C. Linderholm, A. Lyngfelt, Operation of a 100kW chemical-looping combustor with Mexican petroleum coke and Cerrejón coal, Appl. Energy 113 (2014) 1830–1835.
[68] A. Thon, M. Kramp, E.-U. Hartge, S. Heinrich, J. Werther, Operational experience with a system of coupled fluidized beds for chemical looping combustion of solid fuels using ilmenite as oxygen carrier, Appl. Energy 118 (2014) 309–317.
[69] A. Abad, R. Pérez-Vega, L.F. de Diego, F. García-Labiano, P. Gayán, J. Adánez, Design and operation of a 50 kW_{th} Chemical Looping Combustion (CLC) unit for solid fuels, Appl. Energy 157 (2015) 295–303.
[70] J. Ströhle, M. Orth, B. Epple, Chemical looping combustion of hard coal in a 1 MW_{th} pilot plant using ilmenite as oxygen carrier, Appl. Energy 157 (2015) 288–294.
[71] International Organization for Standardization. ISO, 17294-2:2016 Water quality — Application of inductively coupled plasma mass spectrometry (ICP-MS) — Part 2: Determination of selected elements including uranium isotopes, 2016.
[72] T. Mattisson, A. Järdnäs, A. Lyngfelt, Reactivity of some metal oxides supported on alumina with alternating methane and oxygen–application for chemical-looping combustion, Energy Fuel 17 (2003) 643–651.
[73] A. Lyngfelt, B. Leckner, A 1000 MW_{th} boiler for chemical-looping combustion of solid fuels – Discussion of design and costs, Appl. Energy 157 (2015) 475–487.
[74] A. Cuadrat, A. Abad, F. García-Labiano, P. Gayán, L.F. de Diego, J. Adánez, The use of ilmenite as oxygen-carrier in a 500 W_{th} Chemical-Looping Coal Combustion unit, Int. J. Greenhouse Gas Control 5 (2011) 1630–1642.

[75] H. Leion, A. Lyngfelt, M. Johansson, E. Jerndal, T. Mattisson, The use of ilmenite as an oxygen carrier in chemical-looping combustion, Chem. Eng. Res. Des. 86 (2008) 1017–1026.
[76] N. Berguerand, A. Lyngfelt, Design and operation of a 10kW$_{th}$ chemical-looping combustor for solid fuels – Testing with south African coal, Fuel 87 (2008) 2713–2726.
[77] F. Johnsson, A. Vrager, B. Leckner, Solids flow pattern in the exit region of a CFB-furnace - influence of exit geometry, in: 15th International Conference on Fluidized Bed Combustion, Savannah, USA, 1999.
[78] P. Cho, T. Mattisson, A. Lyngfelt, Comparison of iron-, nickel-, copper- and manganese-based oxygen carriers for chemical-looping combustion, Fuel 83 (2004) 1215–1225.
[79] D. Mei, H. Zhao, S. Yan, Kinetics model for the reduction of Fe_2O_3/Al_2O_3 by CO in Chemical Looping Combustion, Chem. Eng. Process. Process Intensif. 124 (2018) 137–146.
[81] D. Mei, A. Abad, H. Zhao, S. Yan, B. Wang, Q. Yuan, Extension and evaluation of a macroscopic model for syngas-fueled chemical looping combustion, Chem. Eng. Process. Process Intensif. 133 (2018) 106–116.
[82] M. Kramp, A. Thon, E.-U. Hartge, S. Heinrich, J. Werther, Carbon Stripping – a critical Process step in Chemical Looping Combustion of Solid Fuels, Chem. Eng. Technol. 35 (2012) 497–507.
[83] C. Linderholm, P. Knutsson, M. Schmitz, P. Markström, A. Lyngfelt, Material balances of carbon, sulfur, nitrogen and ilmenite in a 100kW CLC reactor system, Int. J. Greenhouse Gas Control 27 (2014) 188–202.